Crystallization and Microstructure of Poly(L-lactide-*co*-*meso*-lactide) Copolymers

Jiang Huang,† Melissa S. Lisowski, and James Runt*

Department of Materials Science & Engineering, The Pennsylvania State University, University Park, Pennsylvania 16802

Eric S. Hall, Robert T. Kean, and Nancy Buehler

Central Research & Eco-PLA, Cargill Inc., Minneapolis, Minnesota 55440

J. S. Lin

Solid State Division, Oak Ridge National Laboratory, Oak Ridge, Tennessee 37831

Received October 6, 1997; Revised Manuscript Received January 27, 1998

ABSTRACT: Small-angle X-ray scattering (SAXS), optical microscopy and differential scanning calorimetry were used to establish relationships between crystallization, microstructure, and equilibrium melting temperature (T_m^0) for random copolymers of poly(L-lactide-*co*-*meso*-lactide). T_m^0s derived using the Gibbs−Thomson and data-fitting[23] approaches were found to be in excellent agreement and decreased significantly with increasing *meso*-lactide concentration. Analysis of these equilibrium melting temperatures using models for copolymer crystallization leads to the conclusion that the meso defects are rejected from the crystalline regions. From analysis of the SAXS data, it was concluded that the copolymers contained significant interfibrillar regions whose concentration increased with higher comonomer content. Spherulitic growth rates were strongly dependent on meso content and were analyzed using the Lauritzen−Hoffman kinetic theory of crystal growth.

1. Introduction

Interest in polylactides has rapidly grown in recent years due to their biodegradability and biocompatibility.[1−3] Studies have shown that their biodegradability varies dramatically with chemical composition, e.g., poly(L-lactide) and poly(D-lactide) degrade slowly, while copolymer polylactides degrade much faster, the rate increasing with increasing comonomer concentration.[4,5] To utilize this in the development of environmental-friendly materials, the understanding of polylactide copolymers is critical. Among the various polylactides, poly(L-lactide), poly(D-lactide), and the stereocomplex of these have been widely studied[6−10] but relatively little attention has been paid to poly(L-lactide-*co*-*meso*-lactide)—the polylactide material containing meso segments (D,L-diastereoisomer). Earlier studies[1,11,12] have shown that the concentration of meso segments in the poly(L-lactide-*co*-*meso*-lactide) strongly influences the observed melting temperature and crystallization rate. In the present investigation we explore the crystallization kinetics, microstructure, and equilibrium melting behavior of melt-crystallized poly(L-lactide-*co*-*meso*-lactide)s as a function of optical composition and compare the observed behavior to that predicted by models for random copolymer crystallization.

2. Experimental Section

Materials. The poly(L-lactide-*co*-*meso*-lactide) samples used in this study were synthesized by melting and mixing L-lactide (Boehringer-Ingelheim) and *meso*-lactide (Purac Biochem) in a flask under nitrogen. Tin(II) octanoate was added (molar ratio 10,000:1 lactide to tin) and the mixture transferred to silanized glass vials. The components were then polymerized at 180 °C for 4 h. The copolymers were then dissolved in dichloromethane, filtered, and precipitated from methanol. The samples were dried under vacuum overnight to constant weight. Previous studies have shown that these copolymers are essentially random.[11]

The molecular weights of the polymers were determined by gel permeation chromatography using Waters Ultrastyragel columns and tetrahydrofuran as the mobile phase, against polystyrene standards. The molecular weight, meso concentration in the polymerization and D isomer content (determined by chiral liquid chromatography) are listed in Table 1. Since the molecular weights of all polymers in Table 1 are identical within experimental error, differences in crystallization kinetics can be attributed directly to differences in optical concentration. Compositions are in either mole (or equivalently) weight percent.

Spherulitic Growth Rate Measurements. The synthesized samples were further dried at 80 °C for 48 h in a vacuum oven and then the dried poly(L-lactide-*co*-*meso*-lactide) powder was melted between two cover slips, approximately 30 °C above the observed sample melting temperature in a Mettler hot stage (model FP-82) for 3 min to erase previous thermal history. A pair of tweezers was used to press the top cover slip gently so that the thickness of the samples is thin enough for optical microscope studies. The samples were then quenched to the desired isothermal crystallization temperature (T_x). At higher crystallization temperatures, however, due to the extremely slow nucleation rate, a self-seeding technique was used to accelerate the nucleation process. In this case, the molten samples were first quenched to a lower crystallization temperature [where sizable spherulites (∼50 μm) would appear within 15 to 30 min]. The samples were then heated to the desired T_x and growth rates were recorded after the samples remained at that temperature for 15 min. Our experiments showed that growth rates measured using this method are identical to those without self-seeding. An Olympus intervalometer and an RCA VCR (NSIA) were added to the microscope

* To whom correspondence should be addressed.
† Present address: Caterpillar, Inc.—CPBU, P.O. Box 4000, Bldg. H2000, Mossville, IL 61552.

S0024-9297(97)01462-9 CCC: $15.00
Published on Web 03/24/1998

Table 1. Characteristics of Poly(L-lactide-*co*-*meso*-lactide) Copolymers

sample ID	meso %	$\bar{M}_n$	$\bar{M}_w$	d %
A		65 500	127 400	0.4
B	3	65 800	122 600	2.1
C	6	63 900	119 100	3.4
D	12	65 500	121 300	6.6

setup (Olympus BHSP-300) to record the growth of the spherulites. The radii of the spherulites as a function of time, temperature, and meso concentration were measured directly from the monitor screen, whose scale was calibrated with a Fisher stage micrometer. Reported spherulitic growth rates (G) were determined as the mean of the rates from 1−17 spherulites (average ∼7), monitored on from one to three samples.

Differential Scanning Calorimetry. Differential scanning calorimetry (DSC) melting studies were carried out on a Perkin-Elmer DSC model 7 at 10 °C/min under nitrogen flow. Samples were cut to nearly identical shape and weight, and the sample weight was maintained at very low levels (0.15 ± 0.05 mg) to minimize thermal lag during the DSC heating scan. Melting temperatures were calibrated with indium and tin standards and are reported at the peak in the melting endotherm. DSC experiments reveal that the T_g of the poly(L-lactide-*co*-*meso*-lactide) samples is independent of meso concentration for the polymers considered here ($T_g \sim 57$ °C) and the crystallization window narrows significantly with increasing meso content in the copolymer. If a fraction of the D units are incorporated in the crystals, the equilibrium heat of fusion (ΔH_f^0) will be a function of D isomer content.[13] However, the decrease in ΔH_f^0 would be expected to be only a few percent, even at the highest D isomer concentrations considered here. Therefore, ΔH_f^0 for poly(L-lactide) was used in all cases to convert measured heats of fusion to bulk crystallinities (φ_c). There is some ambiguity in ΔH_f^0 reported for poly(L-lactide) (see refs 1, 6, and 14−16): we chose a value of 100 J/gm which is derived from slowly polymerized, highly crystalline poly(L-lactide).

Small-Angle X-ray Scattering. The 30 × 30 × 1 mm specimens for small-angle X-ray scattering (SAXS) experiments were prepared in a Mettler hot stage (model FP-82). Samples were first melted at a temperature 40 °C above the observed melting temperature of the polymer and held at that temperature for 5 min. They were then quenched to the desired crystallization temperature. After primary crystallization of the polymer was completed (15 to 960 min, depending on T_x and copolymer composition), all samples were quenched to room temperature.

SAXS experiments were carried out on the Oak Ridge National Laboratory 10 m pinhole-collimated SAXS camera using pyrolytic graphite-monochromatized Cu Kα radiation (λ = 0.154 nm) and a 20 × 20 cm^2 position-sensitive area detector with 1 mm resolution. Scattered intensities were stored in a 64 × 64 array. Calibrations were made for instrumentation background and detector efficiency with a ^{55}Fe radioactive standard on a cell-by-cell basis. Each specimen was measured at sample-to-detector distances of 2.119 and 5.119 m to extract data at high and low scattering angles, respectively. The data were azimuthally averaged in the respective high and low q ranges, q = 0.104 to 2.645 nm^{-1} and q = 0.041 to 1.086 nm^{-1} (q is the scattering vector, $q = (4\pi/\lambda)\sin(\theta/2)$, θ is the scattering angle, and λ is the X-ray wavelength). The data were converted to an absolute differential cross-section (cm^{-1} units) by means of precalibrated secondary standards: a high-density polyethylene secondary standard, PES-3, was used for the low q data and a vitreous carbon standard was employed for the high q data. For each sample, high q data were suitably appended to the low q data, and the scattered intensities were corrected for electronic noise. Intensities were truncated at $q \approx 0.09$ nm^{-1} as scatter from the beam stop was observed at lower angles.

The analysis of the SAXS intensity curve based upon the one-dimensional electron density correlation function has been given by Vonk and Kortleve[17] and Strobl et al.[18] The correlation function [$G(r)$] is calculated as

$$G(r) = \left(\frac{1}{2\pi}\right)^2 \int q^2 I(q) \cos(qr)\, dq \qquad (1)$$

where $I(q)$ is the experimental SAXS intensity corrected for thermal fluctuations and r is the correlation distance. A pseudo-two-phase model was applied to the correlation functions of poly(L-lactide-*co*-*meso*-lactide) samples. Figure 1 illustrates a typical one-dimensional correlation function for one of the samples under investigation. The average long period, L_{cor}, can be determined from the first maximum of the correlation curve. When the linear crystallinity is greater than 0.5, the intersection of the linear fit to the self-correlation portion of $G(r)$, $(dG/dr)_{fit}$, with $G(r) = 0$ is r_0

$$r_0 = l_c(1 - w_c) \qquad (2)$$

and therefore

$$r_0/L_{cor} = w_c(1 - w_c) \qquad (3)$$

where w_c is the linear crystallinity (defined as the ratio of the average lamellar thickness l_c to the average long period, L_{cor}). For $w_c < 0.5$, w_c is replaced by $(1 - w_c)$ in the above expressions. We followed the procedures described in Talibuddin et al.[19] for determination and analysis of $G(r)$ and interested readers should see that paper for additional details. Further discussion of determination of l_c and l_a (the average amorphous layer thickness in lamellar stacks) can be found in the next section.

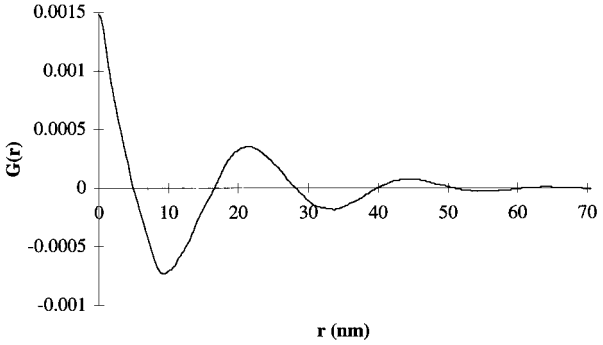

Figure 1. Typical one-dimensional correlation function (for material D: T_x = 113 °C, t_x = 720 min).

3. Results and Discussion

Bulk Crystallinity. Degrees of crystallinity for the four copolymers are seen in Figure 2 plotted as a function of the degree of supercooling ($\Delta T = T_m° - T_x$, where $T_m°$ is the equilibrium melting point of the copolymer in question). At constant ΔT, φ_c decreases dramatically with increasing D isomer content, ranging from ca. 40−60% for material A to values <20% for copolymer D (containing 6.6% D isomer). In addition, φ_c increases with decreasing ΔT, except for material D where it remains constant over the ΔT range investigated. This behavior is very similar to that reported by Cheng et al. for polypropylenes of different isotacticity.[20]

Microstructure. Smoothed and Lorentz-corrected SAXS profiles of sample A crystallized isothermally at selected temperatures are shown in Figure 3. The shift in the first-order maximum, q_{max}, to smaller q (smaller angles) with increasing T_x is consistent with the generally expected increase in long spacing with decreasing undercooling. Long spacings, L, can be calculated by the Bragg relation, $L = 2\pi/q_{max}$, and are plotted in

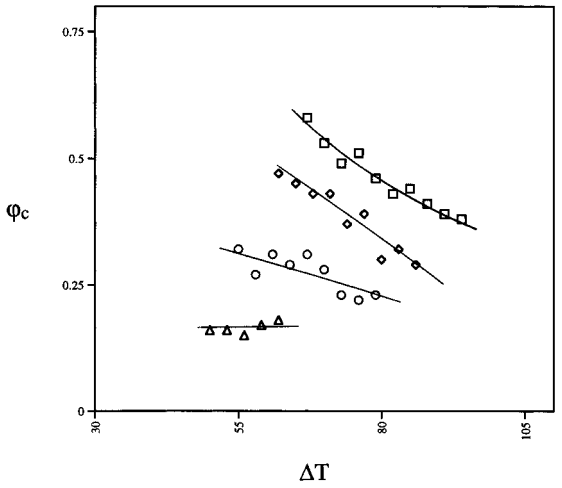

Figure 2. Bulk degrees of crystallinity as a function of degree of supercooling: (□) material A; (◇) material B; (○) − material C; (△) material D.

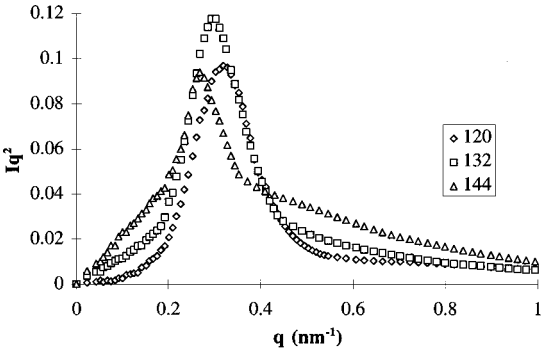

Figure 3. Smoothed and Lorentz-corrected SAXS profiles of selected samples of material A, isothermally crystallized at 120, 132, and 144 °C.

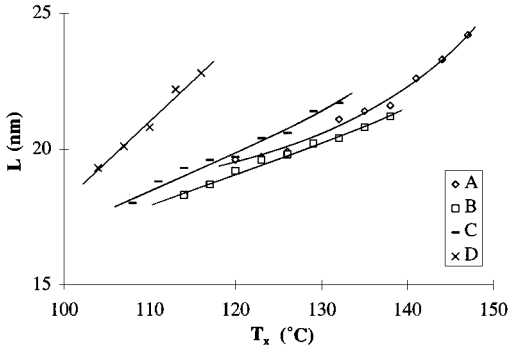

Figure 4. Plot of long spacing as a function of T_x for the four poly(L-lactide-*co*-*meso*-lactide) samples.

Figure 4. As mentioned earlier, the long spacing of the samples can also be obtained from the first correlation function maximum. We found that the values from both methods were nearly identical but those derived from the Lorentz-corrected peak maxima exhibit somewhat greater consistency and were therefore used in the determination of l_c and l_a. Note from Figure 4 that, with the exception of sample A, the long spacing increases with increasing meso concentration. This is consistent with the lower degree of crystallinity at higher meso concentrations.

The bulk crystallinities of the poly(L-lactide-*co*-*meso*-lactide)s under investigation are too low (ca. 15−60%) to confidently assume that the amorphous component is located only within the lamellar stacks (i.e. one cannot

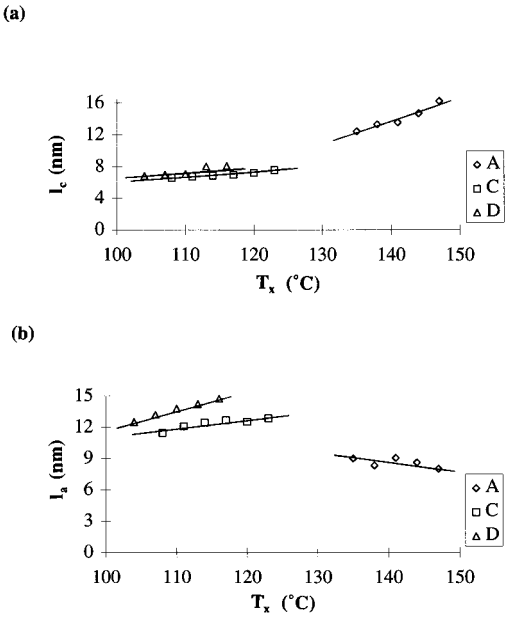

Figure 5. (a) Plot of average lamellar thickness of poly(L-lactide-*co*-*meso*-lactide)s as a function of crystallization temperature. (b) Average amorphous layer thickness in lamellar stacks as a function of crystallization temperature.

a priori assume that the materials are composed of infinite lamellar stacks) and thus the simple relationship $l_c = L\varphi_c$ (where φ_c is the bulk crystallinity) cannot necessarily be used to determine l_c. From our optical microscopy experiments we know that there is no significant amount of material in interspherulitic regions, as all spherulites impinge upon the completion of primary crystallization (for all materials at all T_x considered). By comparing the linear crystallinity derived from the SAXS correlation function and the bulk crystallinity from DSC, one can determine the fraction of the amorphous material residing in interfibrillar regions. From the definition of the linear crystallinity it follows that, $w_c \geq \varphi_c$. The case where $w_c = \varphi_c$ indicates that effectively all of the amorphous component resides in interlamellar regions; i.e., the system consists essentially of continuous lamellar stacks and $l_c = L\varphi_c$. $w_c > \varphi_c$ indicates that a certain amount of the amorphous component resides in interfibrillar regions and the partitioning between the interfibrillar and interlamellar regions can be calculated from w_c and φ_c.

Although one cannot distinguish w_c from w_a ($w_a = 1 - w_c$, the interlamellar amorphous fraction) or l_c from l_a directly from the correlation function, other evidence can assist in doing so. It is well-known that lamellar thickness generally increases with increasing T_x. More importantly, as noted above, $w_c \geq \varphi_c$. Therefore, for example, if the bulk crystallinity of a sample is found experimentally to be 60%, the linear crystallinity should be at least 60%. If the solutions from eq 3 are $w_c = 0.7$ and $w_c = 0.3$, one would therefore conclude that $w_c = 0.7$.

Calculated values for l_c and l_a (from $l_c = Lw_c$, and $l_a = Lw_a$) are plotted in parts a and b, respectively, of Figure 5 against the isothermal crystallization temperature. When using the correlation function and eq 3 to deduce l_c (and consequently l_a) there is considerable uncertainty in estimating w_c, and hence l_c, when the linear crystallinity is near 0.5. Therefore, only w_c data in the range <0.4 or >0.6 were used to calculate the l_c and l_a appearing in Figure 5, and only these data were

Table 2. Linear and Bulk Crystallinities and Percentage of Amorphous Component Residing in Interlamellar Regions for Selected Poly(L-lactide-*co*-*meso*-lactide) Samples

T_x (°C)	copolymer	w_c	ϕ_c	η
138	A	0.62	0.51	0.62
141	A	0.6	0.49	0.63
147	A	0.67	0.58	0.69
108	C	0.37	0.23	0.51
114	C	0.35	0.23	0.56
123	C	0.37	0.29	0.68
104	D	0.35	0.18	0.40
110	D	0.34	0.15	0.34
116	D	0.35	0.16	0.36

used in the Gibbs−Thomson equation (see the following section). Since all calculated linear crystallinities fall in this range for copolymer B, no data for this material appears in Figure 5.

l_c increases with increasing T_x, but its dependence on copolymer meso concentration is difficult to assess due to the modest number of specimens for which l_c can be reliably determined. For both the copolymer inclusion and exclusion models, l_c is predicted to increase with comonomer concentration at a given T_x.[21,22] For example, following the theory of Sanchez and Eby,[22] for the case of complete exclusion of D units (see below), as much as a 20% increase in l_c for copolymer D (6.6% D units) over that of material A would be expected.

As seen in Figure 5b, l_a increases with increasing meso concentration, indicating there is relatively more amorphous material incorporated into lamellar stacks at higher meso levels. From a comparison of the bulk and linear crystallinities in Table 2, clearly not all amorphous material is contained in interlamellar regions; a significant portion resides in interfibrillar regions. Using ϕ_c and w_c listed in Table 2, we can estimate the distribution of the amorphous fraction in the various samples (this could not be done for copolymer B as noted above). The fraction of the amorphous material residing in interlamellar regions, η, can be calculated (η + fraction of the amorphous component residing in interfibrillar regions = 1) and indicates that the fraction of the amorphous component within lamellar stacks decreases with increasing meso concentration. In other words, it appears that there is more interfibrillar material in copolymers of higher comonomer content.

Equilibrium Melting Points. The most popular method for determining equilibrium melting points of polymers is the Hoffman−Weeks approach, derived from eq 4 below and several simplyifying assumptions.[23] The popularity of this approach stems from the need to measure only the experimental melting points, and the apparent ease with which this can be done. However, Hoffman−Weeks plots (T_m vs T_x) are sometimes curved,[24] making unambiguous estimation of $T_m°$ difficult. In fact, Hoffman−Weeks plots for the four poly(L-lactide-*co*-*meso*-lactide) polymers under consideration here exhibit strong curvature at relatively low T_x. Moreover, a recent paper calls into question the use of conventional form of the Hoffman−Weeks expression for polymers displaying low degrees of crystallinity.[25]

The Gibbs−Thomson approach utilizes the rigorous correlation between crystal thickness and crystal stability[23]

$$T_m = T_m°\left[1 - \frac{2\sigma_e}{\Delta H_f^0(l_c)}\right] \qquad (4)$$

Table 3. $T_m°$ and Fold Surface Free Energies Derived from Gibbs-Thomson Analysis, and $T_m°$ from the Data-Fitting Method

sample	$T_m°$ (°C) G−T treatment	σ_e (erg/cm^2)	$T_m°$ (°C) data-fitting treatment
PLLA (lit. value)[6,26]	207−212	61	
A	214	60	215
B			200
C	187	37	192
D	166	27	164

where T_m is the observed melting point for lamella of thickness l_c and σ_e is the fold surface free energy. The equilibrium melting temperatures of the poly(L-lactide-*co*-*meso*-lactide)s were estimated from plots of T_m vs $1/l_c$ and extrapolation to $1/l_c = 0$. Fold surface free energies were extracted from the slope of the linear extrapolations. The results are listed in Table 3, along with literature values for poly(L-lactide) (PLLA).[6,26] $T_m°$ and σ_e for material A, which is essentially PLLA, are very similar to the PLLA literature values. However, since both literature $T_m°$ values were obtained using the Hoffman−Weeks method, they must be viewed with some caution. Since only data where the linear crystallinities are in the range <0.4 or >0.6 are used in the analysis, only five or six data points are available for materials A, C, and D, leading to a statistical uncertainty (standard deviation) on the order of ±10 °C in $T_m°$. As noted above, all linear crystallinities for material B are within 0.4 and 0.6 and no reliable $T_m°$ and σ_e values could be determined using this procedure.

An independent data-fitting method[27,28] was used to verify these estimated $T_m°$. Recently, Huang et al.[27] proposed a method that estimates $T_m°$ directly from growth rate data, using the Lauritzen−Hoffman kinetic model.[23] Specifically, a seed $T_m°$ value is chosen, then the linear regression of

$$\ln G + \frac{U^*}{R(T_x - T_\infty)} \text{ vs } \frac{1}{T_x(\Delta T)f}$$

for each regime is performed using this seed value. U^* is the activation energy for transport of segments across the melt−crystal interface, T_∞ the temperature below which all viscous flow ceases (taken here as $T_g - 30$ K), and f a function which accounts for the temperature dependence of the heat of fusion [$f = 2T_x/(T_m° + T_x)$]. From the linear regression, the values of the slope (K_g) and of the intercept (ln G_0) are obtained. From the Lauritzen−Hoffman kinetic theory[23]

$$\ln G_0 - \frac{K_g}{T_x(\Delta T)f} = \ln G + \frac{U^*}{R(T_x - T_\infty)} \qquad (5)$$

The values of the left-hand side of eq 5 calculated with the initial K_g and ln G_0 are compared to those of the right-hand side (rhs), which are calculated based on the experimentally measured growth rates. The values of the LHS are called linear regression values. These are compared with the RHS values (the "experimental values") and the variance of the fit, s^2, calculated as

$$s^2 = \sum(\text{experimental value} - \text{linear regression value})^2/n - 2 \qquad (6)$$

where n is the number of data points. By varying the value of the trial $T_m°$, one arrives at a minimum

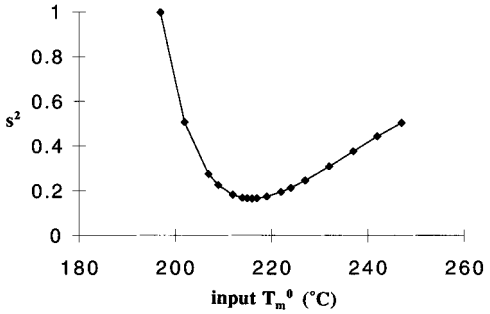

Figure 6. Variance s^2 of the least-squares fit as a function of input $T_m°$ for material A.

variance and the $T_m°$ that results in the minimum variance is taken as the equilibrium melting temperature of the polymer in question. This method has been used successfully on several semicrystalline polymers including poly(pivalolactone) and isotactic poly(styrene).[27−29] See ref 27 for further discussion and precautions for using this approach.

Figure 6 shows the variance of the least-squares fit vs input $T_m°$ for material A. $T_m°$ values determined via this approach are tabulated in Table 3 for the four poly(L-lactide-*co*-*meso*-lactide)s. Note that the values derived independently from the two methods for materials A, C, and D are identical within experimental error. For material B, the data fitting method gives what appears to be a consistent $T_m°$, and we will use this value in our analysis of the spherulitic growth rates. Note that the equilibrium melting temperatures of the copolymers decrease dramatically with increasing meso concentration: from 214 °C for material A to 165 °C for sample D, a decrease of almost 50 °C at 6.6% D optical content.

Several models have been proposed to account for the change in equilibrium melting points of crystalline random copolymers as a function of comonomer concentration.[21,22,30,31] For the case of complete exclusion of comonomer B in a semicrystalline AB random copolymer, Flory showed that[21]

$$\frac{1}{T_m°'} - \frac{1}{T_m°} = \frac{-R}{\Delta H_f°} \ln X_A \tag{7}$$

where $T_m°'$ is the equilibrium melting point of the copolymer and X_A the mole fraction of the crystallizable comonomer. Baur proposed a modification of the Flory model to account for the average sequence length of crystallizable comonomer (ξ) and arrived at[30]

$$\frac{1}{T_m°'} - \frac{1}{T_m°} = \frac{-R}{\Delta H_f°}(\ln X_A - 1/\xi) \tag{8}$$

$\xi = [2X_A(1 - X_A)]^{-1}$ for random copolymers[32] and is estimated to be 24, 15 and 8 for copolymers B through D, respectively (taking the lactic acid unit as repeat unit). For uniform inclusion of comonomer B in A crystals, Sanchez and Eby have shown that[22]

$$T_m°' = T_m° + \left(1 - \frac{\epsilon}{\Delta H_f°} X_B\right) \tag{9}$$

where X_B is the mole fraction of noncrystalline comonomer and ϵ the excess defect free energy.

The predicted $T_m°'$ from both the original Flory exclusion model and the uniform inclusion model (using

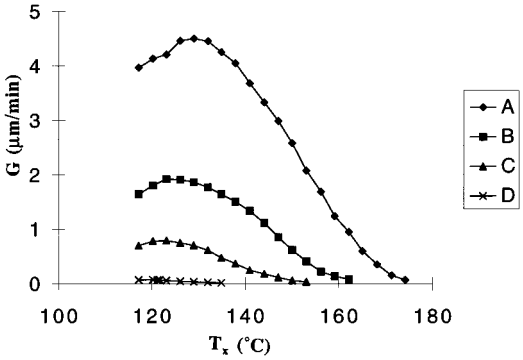

Figure 7. Spherulitic growth rates of poly(L-lactide-*co*-*meso*-lactide) copolymers as a function of crystallization temperature.

Table 4. Equilibrium Melting Point Predictions of Copolymer Models vs Experimentally Derived Values

		mp (°C)			
material	ξ	experimental[a]	Flory[21]	Sanchez-Eby[22]	Baur[30]
B	24	200	209	211	198
C	15	192	206	209	189
D	8	164	197	204	168

[a] From data fitting method.

$\epsilon \approx 35$ J/gm[22]) are much larger than those determined experimentally (see Table 4). Force fitting eq 9 to the data yields an unrealistic value for ϵ ($\sim 1.7\Delta H_f°$), especially considering that the defect units have the same chemical makeup as the crystallizable species. However, the predicted values from the Baur modification of the Flory expression (eq 8) fit the data extremely well, implying exclusion of the D units from the crystals. This result appears initially surprising in that Fischer et al. have concluded that at least some D units are included in the L crystal lattice for solution grown crystals of poly(L-lactide-*co*-*meso*-lactide)s[1]. However, Fischer et al. also found that rejection of D co-units *increased* significantly with increasing ΔT,[1] the opposite of what would be expected based on crystallization kinetics arguments. Our $T_m°'$ values were obtained from experimental melting points derived from crystals formed at relatively high ΔT, and in that sense our results are consistent with those of Fischer et al.[1] In addition, defect exclusion is also consistent with relatively low degrees of crystallinity exhibited by the copolymers. Hydrolysis experiments followed by chiral liquid chromatography are currently being conducted to verify the inferences from the equilibrium melting data.

Crystallization Kinetics. The experimental spherulitic growth rate data are plotted in Figure 7. At a crystallization temperature of 117 °C, the growth rate of material A (0.4% D) is about 60 times faster than that of material D (6.6% D), whereas at 135 °C the dependence of growth rate on meso concentration is much more significant (the ratio of the growth rates of materials A and D is more than 340). This behavior is a manifestation of the reduction in equilibrium melting temperature with meso concentration. Careful consideration of the data also suggests that the temperature where the maximum growth rate occurs is shifted somewhat to lower temperatures with increasing D isomer content (from $T_{Gmax} = 129$ °C for sample A to $T_{Gmax} = 120$ °C for material D). Finally, it is of interest to compare the growth rates of our polylactide copolymers with that of poly(ethylene terephthalate) [PET]. Although the T_g of PET is on same order as that for the

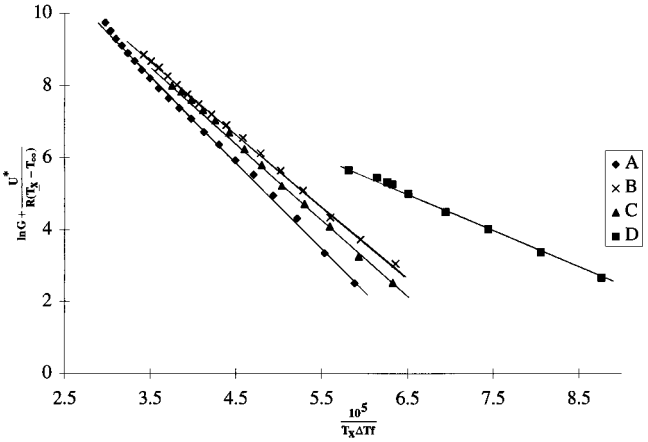

Figure 8. LH plots for the poly(L-lactide-*co*-*meso*-lactide) copolymers.

poly(L-lactide-*co*-*meso*-lactide)s (i.e., ~75 °C), its equilibrium melting point is considerably higher (i.e., 280 °C),[32] resulting in a wider crystallization window. PET of $M_n = 39\ 100$ exhibits a maximum spherulitic growth rate (at ~180 °C) of about 1.5 μm/min[33] compared to maximum values of approximately 4.5, 1.9, 0.8, and 0.07 μm/min, respectively, for poly(L-lactide-*co*-*meso*-lactide)s A through D.

In early work by Andrews et al.,[34] a relationship between the spherultic growth rate, G, and comonomer content at a given T_x was proposed for X_B up to about 10%

$$\ln G \cong -(N-1)\,X_B + \ln G_0' \qquad (10)$$

where G_0' is the spherulite growth rate of the homopolymer and N the critical sequence length for surface nucleation. A similar linear dependence of ln G on X_B is also predicted by the theory of Sanchez and Eby.[22] A linear ln G vs X_B relationship has been found experimentally for different random copolymer systems[34−36] and although we only have three data points at the various T_x values, our data appear to be linear as well. Estimating N from the slope of these plots leads to values on the order of 90 ± 20. Average l_c's for copolymers C and D are ~8 nm at the T_x in question and the length of the PLLA (lactic acid) repeat unit is ~0.29 nm[1], which leads to a critical nucleus of approximately three to four stems. Similar values have been determined for *cis*-polyisoprene[34] and cross-linked polyethylene.[36]

Analysis of spherultic growth was undertaken using the Lauritzen-Hoffman kinetic theory[23,24] using $T_\infty = T_g - 30$ K and $U^* = 1500$ cal/mol (see eq 5). K_g, the nucleation constant, is defined as $K_g = n_i b_0 \sigma \sigma_e T_m^\circ / k\Delta H_f^\circ$, where n_i is 4 for crystallization regimes I and III and 2 for regime II, b_0 is the layer thickness, σ is the lateral surface free energy, and k is the Boltzmann constant.

A plot of ln $G + U^*/R(T_x - T_\infty)$ vs $1/T_x\Delta Tf$ (the so-called LH plot) yields the nucleation constant, K_g (the slope), and ln G_0 (the intercept) (see eq 5). Figure 8 presents the LH plots for the four materials. The following parameters were used in our analysis: $b_0 = 0.517$ nm[6] and crystalline and amorphous densities of 1.29 and 1.25 g/cm^3, respectively[1]. The fitted values for K_g are reported in Table 5. The regime(s) in which growth occurs must be determined before $\sigma\sigma_e$ can be calculated. In contrast to what is reported in the literature, where regime I to II[6] and regime II to III[37] transitions have been reported for PLLA, neither the growth rate nor LH plots (Figures 7 and 8, respectively) exhibit obvious breaks for any of the four poly(L-lactide-*co*-*meso*-lactide)s. We therefore conclude that crystallization takes place in a single growth regime over the range of crystallization temperatures explored here. Lauritzen[38] proposed that the value of K_g can be used to test whether the growth occurs in regime I or II by the application of the Z-test. Z is defined as

$$Z \cong 10^3\left(\frac{L'}{2a}\right)^2 \exp\left(\frac{-X}{T_x\Delta Tf}\right) \qquad (11)$$

where L' is the substrate length and a the chain stem width ($a = 0.594$ nm for PLLA[6]). Regime I kinetics are followed if substitution of $X = K_g$ in the above equation leads to $Z < 0.01$; if with $X = 2K_g$ eq 11 results in $Z > 1$, then regime II growth is indicated. In practice, the Z-test is performed by using the K_g values derived from the LH plots and the inequalities for Z to estimate the range of L' values for regime I or regime II. The regime is then determined by deciding whether the range of L' values calculated in each case is reasonable. However, the difficulty is in determining what constitutes a reasonable value for L' in each regime. Polyethylene is the only polymer for which L' has been estimated and what is considered reasonable at the regime I to II transition has fluctuated over time. A value within a factor of 1.5 of ~87 nm is the most recent estimate.[24] Testing the data for conformity to regime I results in required substrate lengths of ~0.1 nm to about 4.5 nm, with most data around 1 ~ 2 nm, which is unrealistically small (assuming of course that L' values for polylactides are roughly similar to polyethylene). Testing for regime II produced mixed results: at lower T_xs, L' values are "reasonable" (around 40 nm) while at the highest T_xs the calculated L' values appear to be too high (ca. 20 μm). From the Z-tests and the relatively large undercoolings at which the polymers were crystallized, regime I can be ruled out. Unfortunately, there is no clear way to distinguish regime II and III crystallization unless there is a break in the growth rate data. However, since a regime I to II transition has been observed for PLLA with molecular weight close to that of the materials under investigation here[6] and much of our experimental data falls into the range described as regime II, as well as some indications from Z-tests, we chose regime II for the following analysis.

Table 5. Results from Analysis of Kinetic Data

sample	$K_{g(ii)} \times 10^{-5}$ (K^2)	$\sigma\sigma_e$ (erg^2/cm^4)	σ_e (erg/cm^2)	σ (erg/cm^2)
lit values (PLLA)[6,39]	2.29−2.44	733 (av)	61	12
A	2.4	730	60	12
B	2.0	630	45[a]	12
C	2.1	670	37	18
D	1.1	360	27	13

[a] This value was estimated from the slope of the fit of $1/l_c$ through $T_m^\circ = 200$ °C.

The results of the LH analysis (employing T_m°s from the data fitting method) can be found in Table 5. Using σ_e from the Gibbs−Thomson analysis, the lateral surface free energy can be calculated as well. σ and σ_e for material A are nearly identical to the values reported by Vasanthakumar and Pennings[6] and are very close to those derived from a reanalysis of that data by

Hoffman et al.[39] ($K_{g(II)} = 2.44 \times 10^5$ and $\sigma_e = 53 \pm 4$ erg·cm^{-2}). The uncertainty (standard deviation) associated with the slope of our experimental Gibbs−Thomson plots is approximately 10%, and so our results indicate that σ_e decreases with increasing meso concentration and, except for material C, the lateral surface free energy of poly(L-lactide-*co*-*meso*-lactide) is constant, independent of meso concentration. The seemingly anomalous lateral surface free energy for material C very likely arises from experimental uncertainty.

Why might σ_e change significantly with comonomer concentration? As an example, consider the copolymer containing 6.6% D isomer co-units. As noted earlier, the average sequence length of crystallizable L units in this copolymer is about 8, leading to an average length of ~2.4 nm, considerably smaller than the measured lamellar thickness (6−8 nm). Given that the D units are rejected from the crystals, it follows that only the relatively high end of the distribution of L sequence lengths are capable of crystallizing under the conditions used here. This is consistent with the relatively low degree of crystallinity of this copolymer. In the case where a crystal stem of this copolymer attaches at the growth front, it is relatively unlikely that the L sequence length will be long enough to fold and deposit a second stem without encountering another D unit. Therefore, the probability of forming a fold and reentering the crystal is expected to decrease. The fold surface free energy is normally associated with the work of chain folding,[23] but in the case where folding decreases, one would expect σ_e to decrease as comonomer content increases and ultimately approach σ.

Acknowledgment. We would like to express our appreciation to the Advanced Technology Program of NIST for their support of this work (Contract No. 70NANB5H1059). This research was also supported in part by the Division of Materials Sciences, U.S. Department of Energy, under Contract No. DE-AC05-96OR22464 with Lookhead Martin Energy Research Corporation. Finally, we would also like to thank Dr. Sapna Talibuddin and Dr. Jeffrey Kostad for helpful discussions.

References and Notes

(1) Fischer, E. W.; Sterzel, H. J.; Wegner, G. *Kolloid Z. Z. Polym.* **1973**, *251*, 980.
(2) Reed, A. M.; Gilding, D. K. *Polymer* **1981**, *22*, 494.
(3) Leenslag, J. W.; Pennings, A. J.; Bos. R. R. M.; Rozema, F. R.; Boering, G. *Biomaterials* **1987**, *8*, 311.
(4) Pitt, C. G.; Gu, Z. *J. Controlled Release* **1987**, *4*, 283.
(5) Miller, R. A.; Brady, J. M.; Cutright, D. E. *J. Biomed. Mater. Res.* **1977**, *11*, 711.
(6) Vasanthakumar, R.; Pennings, A. J. *Polymer*, **1983**, *24*, 175.
(7) Jamishidi, K.; Hyon, S.-H.; Ikada, Y. *Polymer*, **1988**, *29*, 2229.
(8) Kalb, B.; Pennings, A. J. *Polymer*, **1980**, *21*, 607.
(9) Tsuji, H.; Ikada, Y. *Macromolecules* **1993**, *26*, 6918.
(10) Reeve, M. S.; McCarthy, S. P.; Downey, M. J.; Gross, R. A. *Macromolecules* **1994**, *27*, 825.
(11) Kolstad, J. L. *J. Appl. Polym. Sci.* **1996**, *62*, 1079.
(12) Huang, J.; N. Buehler, N.; Hall, E.; Kean, R.; Kolstad, J.; Wu, L.; Runt, J. *ACS Polymer Preprints* **1996**, *37*, 370.
(13) Sanchez, I. C.; Eby, R. K. *J. Res. NBS* **1973**, *77A*, 353.
(14) Gilding, D. K.; Reed, A. M. *Polymer* **1979**, *20*, 1459.
(15) Cohn, D.; Younes, H.; Marom, G. *Polymer* **1987**, *28*, 2018.
(16) Loomis, G. L.; Murdoch, J. R.; Gardner, K. H. *ACS Polymer Preprints* **1990**, *31(2)*, 55.
(17) Vonk, C. G.; Kortleve, G. *Kolloid Z. Z. Polym.* **1967**, *220*, 19.
(18) Strobl, G. R.; Schneider, M. J.; Voigt-Martin, I. G. *J. Polym. Sci., Polym. Phys. Ed.* **1980**, *18*, 1361.
(19) (a) Talibuddin, S.; Wu, L.; Runt, L.; Lin J. S. *Macromolecules*, **1996**, *29*, 7527. (b) Talibuddin, S. Ph.D. Thesis, The Pennsylvania State University, 1997.
(20) Cheng, S. Z. D.; Janimak, J. J.; Zhang, A.; Hsieh, E. T. *Polymer* **1981**, *32*, 648.
(21) Flory, P. J. *Trans. Faraday Soc.* **1955**, *51*, 848.
(22) Sanchez, I. C.; Eby, R. K. *Macromolecules* **1975**, *8*, 638.
(23) Hoffman, J. D.; Davis, G. T.; Lauritzen, J. I., Jr. in *Treatise on Solid State Chemistry* (Hanny, N. B., Ed.), Vol. 3, Plenum Press: New York, 1976, Chapter 7.
(24) Hoffman, J. H.; Miller, R. L. *Polymer* **1997**, *38*, 3151.
(25) Srinivas, S.; Marand, H. Mauscript in preparation.
(26) Tsuji, H.; Ikada, Y. *Polymer* **1995**, *36*, 2709.
(27) Huang, J. Prasad, A.; Marand, H. *Polymer* **1994**, *35*, 1896.
(28) Huang, J.; Marand, H. *Macromolecules* **1997**, *30*, 1069.
(29) Iler, H. D. Ph.D. Thesis, Virginia Institute of Technology and State University, Blacksburg, VA, 1995.
(30) Baur, H. *Makromol. Chem.* **1966**, *98*, 297.
(31) Helfand, E.; Lauritzen, J. I. *Macromolecules* **1973**, *6*, 631.
(32) Wunderlich, B. *Macromolecular Physics*, Academic Press: New York, 1980; Vol. 3.
(33) van Antwerpen, F.; van Krevelen, D. W. *J. Polym. Sci., Polym. Phys. Ed.* **1972**, *10*, 2423.
(34) Andrews, E. H.; Owen, P. J.; Singh, A. *Proc. R. Soc. London A* **1971**, *324*, 79.
(35) Rensch, G. J.; Phillips, P. J.; Vatansever, N.; Gonzalez, V. A. *J. Polym. Sci., Polym. Phys. Ed.* **1986**, *24*, 1943.
(36) Phillips, P. J.; Lambert, W. S. *Macromolecules* **1990**, *23*, 2075.
(37) Mazzullo, S.; Paganetto, G.; Celli *Colloid Polym. Sci.* **1992**, *87*, 32.
(38) Lauritzen, J. I., Jr. *J. Appl. Phys.* **1973**, *44*, 4353.
(39) Hoffman, J. D.; Miller, R. L.; Marand, H.; Roitman, D. B. *Macromolecules* **1992**, *25*, 2221.

MA9714629